

Tuning and Probing the Distribution of Cu^+ and Cu^{2+} Trap States Responsible for Broad-Band Photoluminescence in CuInS_2 Nanocrystals

Van Der Stam, Ward; De Graaf, Max; Gudjonsdottir, Solrun; Geuchies, Jaco J.; Dijkema, Jurgen J.; Kirkwood, Nicholas; Evers, Wiel H.; Longo, Alessandro; Houtepen, Arjan J.

DOI

[10.1021/acsnano.8b05843](https://doi.org/10.1021/acsnano.8b05843)

Publication date

2018

Document Version

Final published version

Published in

ACS Nano

Citation (APA)

Van Der Stam, W., De Graaf, M., Gudjonsdottir, S., Geuchies, J. J., Dijkema, J. J., Kirkwood, N., Evers, W. H., Longo, A., & Houtepen, A. J. (2018). Tuning and Probing the Distribution of Cu^+ and Cu^{2+} Trap States Responsible for Broad-Band Photoluminescence in CuInS_2 Nanocrystals. *ACS Nano*, 12(11), 11244-112253. <https://doi.org/10.1021/acsnano.8b05843>

Important note

To cite this publication, please use the final published version (if applicable).
Please check the document version above.

Copyright

Other than for strictly personal use, it is not permitted to download, forward or distribute the text or part of it, without the consent of the author(s) and/or copyright holder(s), unless the work is under an open content license such as Creative Commons.

Takedown policy

Please contact us and provide details if you believe this document breaches copyrights.
We will remove access to the work immediately and investigate your claim.

Tuning and Probing the Distribution of Cu^+ and Cu^{2+} Trap States Responsible for Broad-Band Photoluminescence in CuInS_2 Nanocrystals

Ward van der Stam,^{*,†} Max de Graaf,[†] Solrun Gudjonsdottir,[†] Jaco J. Geuchies,[†] Jurgen J. Dijkema,[†] Nicholas Kirkwood,[†] Wiel H. Evers,[†] Alessandro Longo,^{‡,§} and Arjan J. Houtepen^{*,†}

[†]Optoelectronic Materials Section, Faculty of Applied Sciences, Delft University of Technology, van der Maasweg 9, 2629 HZ Delft, The Netherlands

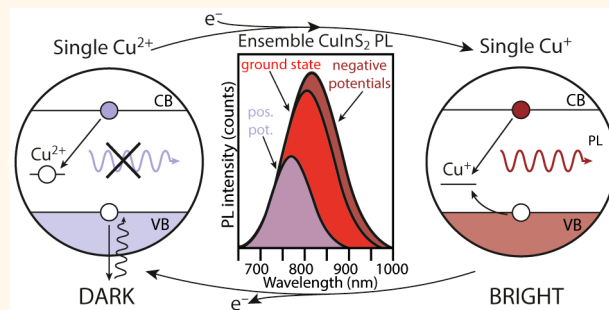
[‡]Netherlands Organization for Scientific Research (NWO), Dutch-Belgian Beamline, ESRF, The European Synchrotron, CS40220, 38043, 71 Avenue des Martyrs, 38000 Grenoble, France

[§]Istituto per lo Studio dei Materiali Nanostrutturati (ISMN)-CNR, UOS Palermo, Via Ugo La Malfa, 153, 90146 Palermo, Italy

Supporting Information

ABSTRACT: The processes that govern radiative recombination in ternary CuInS_2 (CIS) nanocrystals (NCs) have been heavily debated, but recently, several research groups have come to the same conclusion that a photoexcited electron recombines with a localized hole on a Cu-related trap state. Furthermore, it has been observed that single CIS NCs display narrower photoluminescence (PL) line widths than the ensemble, which led to the conclusion that within the ensemble there is a distribution of Cu-related trap states responsible for PL. In this work, we probe this trap-state distribution with *in situ* photoluminescence spectroelectrochemistry. We find that Cu^{2+} states result in individual “dark” nanocrystals, whereas Cu^+ states result in “bright” NCs. Furthermore, we show that we can tune the PL position, intensity, and line width in a cyclic fashion by injecting or removing electrons from the trap-state distribution, thereby converting a subset of “dark” Cu^{2+} containing NCs into “bright” Cu^+ containing NCs and *vice versa*. The electrochemical injection of electrons results in brightening, broadening, and a red shift of the PL, in line with the activation of a broad distribution of “dark” NCs (Cu^{2+} states) into “bright” NCs (Cu^+ states) and a rise of the Fermi level within the ensemble trap-state distribution. The opposite trend is observed for electrochemical oxidation of Cu^+ states into Cu^{2+} . Our work shows that there is a direct correlation between the line width of the ensemble $\text{Cu}^+/\text{Cu}^{2+}$ trap-state distribution and the characteristic broad-band PL feature of CIS NCs and between Cu^{2+} cations in the photoexcited state (bright) and in the electrochemically oxidized ground state (dark).

KEYWORDS: spectroelectrochemistry, copper indium sulfide, trap state, *in situ* X-ray absorption, nanocrystal



Interest in ternary CuInS_2 (CIS) nanocrystals (NCs) as less-toxic alternatives for cadmium-containing NCs has increased considerably over the past few years.^{1–5} Based on the synthetic methodology, *i.e.*, direct synthesis^{6,7} or cation exchange in template $\text{Cu}_2\text{-xS}$ nanocrystals,^{8,9} quasi-spherical NCs with the chalcopyrite crystal structure, or anisotropic morphologies with the wurtzite crystal structure,^{10,11} can be easily obtained. Regardless of the crystal structure or the morphology, ternary CIS nanocrystals are characterized by a large global Stokes shift, long carrier lifetimes and a broad photoluminescence (PL) band.^{3,12–14} Several mechanisms for the radiative recombination in ternary CIS NCs have been

proposed over the years, but recently, a number of research groups have come to the same conclusion that radiative recombination is dominated by a hole on a localized in-gap state and a delocalized conduction band (CB) electron.^{12–15} Furthermore, single NC spectroscopy experiments by the Klimov group¹⁴ and the Gamelin group¹² indicate that the PL line width of individual CIS NCs is narrower than the

Received: August 1, 2018

Accepted: October 29, 2018

Published: October 29, 2018

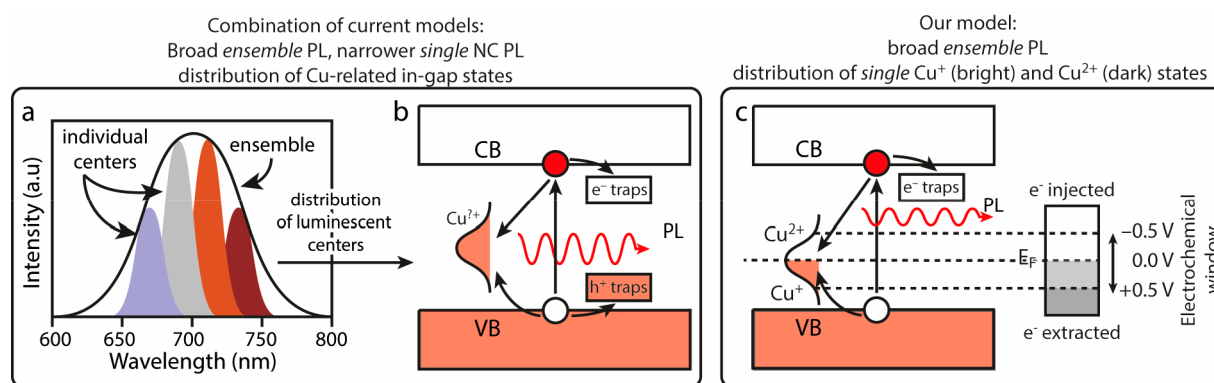


Figure 1. Schematics showing the models for radiative recombination in ternary CuInS₂ nanocrystals, where (a) individual nanocrystals have narrower PL line widths than the ensemble, which is characterized by a broad PL line width. (b) This broad PL line width is hypothesized to correspond to a distribution of Cu-related trap states. The hole and electron traps within the band gap compete with the radiative recombination on the Cu-related defect states and, hence, result in the quenching of the PL. (c) Our model for radiative recombination in ternary CIS NCs involves radiative Cu⁺ defects (below the Fermi level, E_F) and non-radiative Cu²⁺ defect states (above E_F). Nanocrystals that contain a single Cu²⁺ state are “dark”. Surface electron traps within the band gap have a detrimental effect on the PLQY of ternary NCs as well. The distribution of single “bright” Cu⁺ (below E_F) and “dark” Cu²⁺ (above E_F) centers within the ensemble can be tuned by an electrochemical potential.

ensemble PL (Figure 1a), although their interpretation of the reason behind the narrower single NC PL differs. The Klimov group proposed that individual CIS NCs contain luminescent Cu-related defects within the band gap with a slightly different position with respect to the band edges, giving rise to narrow single NC PL but broad ensemble PL. In contrast, the Gamelin group states that the single NC PL is narrower than the ensemble but still significantly broadened compared to typical excitonic PL as a result of the formation of a self-trapped exciton and corresponding strong electron–phonon coupling.^{12,14} Recently, de Mello-Donegá and co-workers have shown with transient absorption spectroscopy that the process of light emission proceeds *via* quick localization of the photogenerated hole on the luminescent defect,¹³ as was also suggested by others.¹⁶ These examples show that the peculiar photophysics of CIS NCs are still heavily debated despite the consensus about the existence of midgap states that quickly localize the photogenerated holes and result in radiative recombination with the delocalized conduction band electron.

Figure 1 schematically shows a combination of the current models for radiative recombination in ternary CIS NCs in which each individual CIS NC displays a narrower PL band than the ensemble at a slightly different wavelength. This is either due to a transition involving a Cu-related defect with a different position with respect to the band edges or due to a self-trapped exciton in combination with varying degrees of electron–phonon coupling, as discussed above (Figure 1a,b).^{16–18} This results in a trap-state distribution for the ensemble PL, whereas individual NCs have narrower PL line widths with slightly different PL wavelengths (Figure 1a,b).^{12,14} After photoexcitation, the photexcited electron radiatively recombines with a rapidly trapped hole, which is localized on the Cu-related state within the trap-state distribution (Figure 1b). However, the exact nature, and especially the oxidation state, of this Cu-related state is heavily debated. It has been proposed that both Cu²⁺ and Cu⁺ trap states are present in CIS NCs and result in photoluminescence, albeit *via* different recombination pathways.^{12,14–19} We will first assume that indeed both Cu⁺ and Cu²⁺ are present (Figure 1b) and intend to validate this hypothesis by *in situ* spectroelectrochemistry.

Recently, two research groups presented changes of the PL in ternary CIS NCs as a function of an applied electrochemical potential.^{17,20} They both observed brightening and darkening of the PL band, which was attributed to a competition between the radiative transition of the delocalized electron in the CB to the localized hole on the Cu defect, with hole and electron trapping in band-gap states near the CB and valence band (VB) edges (Figure 1b).^{17,20} These band-gap states are inferred to originate from surface defects²¹ because the overgrowth of a wide band-gap shell results in reduced dependence of the PL intensity on the applied potential and an increase in the steady-state PL intensity.^{17,20} While surface defects have a detrimental influence on the PLQY of ternary nanomaterials, they are not the only source of non-radiative recombination that needs to be considered because unity PLQY values are not reached upon epitaxial shell overgrowth.^{6,7} Klimov and co-workers also discussed the differences between radiative recombination on Cu⁺ centers, which they conclude is dominant in stoichiometric CIS NCs and is largely influenced by both electron and hole trapping, and on Cu²⁺ centers, which they believe to dominate in Cu deficient samples.²⁰ A complication in their discussion is that it requires the assumption that Cu²⁺ and Cu⁺ ions are not in electrochemical equilibrium and their ratio is not affected by changing the Fermi level electrochemically. Although hole/electron trapping at surface defects clearly affects the PL intensity, which can be tuned by raising the Fermi level,^{17,20} the oxidation of Cu⁺ to Cu²⁺ can also explain the spectroelectrochemical brightening and darkening trends, as we will discuss below.

Here, we probe the nature of the trap-state distribution with *in situ* photoluminescence spectroelectrochemistry and *in situ* X-ray absorption measurements and correlate it to the characteristic optical features of ternary nanomaterials (*i.e.*, broad-band and low-intensity PL). Specifically, we observe a shift and PL line width broadening and narrowing upon raising and lowering the Fermi level, which cannot be explained by reduced electron and hole trapping only. We find that we can activate the individual luminescent centers by injecting electrons into the trap-state distribution (*i.e.*, reducing some of the NCs), thereby converting single NCs containing “dark”

Cu^{2+} centers into “bright” Cu^+ centers, which effectively switches some NCs within the ensemble in the “on” state. *Vice versa*, oxidizing some of the NCs results in deactivation of the bright Cu^+ centers, which switches some NCs into the “off” state. Activation of the luminescent Cu^+ centers results in photobrightening of the ensemble PL (by $\sim 15\%$) but also in a shift to lower energies and a broadening of the PL band. Deactivation results in the opposite: quenching of the PL (by $\sim 55\%$), a shift to higher energies of the PL maximum, and narrowing of the ensemble PL. Interestingly, the shift and changes in the PL line width have not been observed before and are in perfect agreement with a shift of the Fermi level (E_F) within an ensemble distribution of individual “bright” Cu^+ (below E_F) and “dark” Cu^{2+} (above E_F) centers (Figure 1c). These results show that the broad PL line width in ternary CIS NCs indeed correlates with the *ensemble* distribution of trap states within the band gap. In the excited state, photogenerated holes oxidize Cu^+ centers to Cu^{2+} , followed by efficient luminescence. However, the electrochemical oxidation of Cu^+ to Cu^{2+} results in “dark” NCs. This apparent discrepancy is explained by the presence of the photogenerated hole in the valence band (VB) in the case of electrochemically oxidized Cu^{2+} centers. This photogenerated hole provides a pathway for fast nonradiative Auger trapping on the Cu^{2+} defect, effectively quenching the luminescence. Our results indicate that there is a direct correlation between the presence of Cu^{2+} and the characteristic optical properties of ternary CIS NCs, like relatively low PL quantum yield, large global Stokes shift, and broad-band photoluminescence, which can be tuned by electrochemical injection and extraction of electrons.

RESULTS AND DISCUSSION

Synthesis and Characterization of CuInS_2 Nanocrystals. The CuInS_2 (CIS) nanocrystals were characterized with optical spectroscopy (Figure S1), transmission electron microscopy (TEM, Figure S2) and X-ray diffractometry (XRD, Figure S3). These measurements indicate that CIS NCs of 2.9, 3.4, 3.7, and 5.5 nm with the chalcopyrite crystal structure were successfully synthesized. Photoluminescence quantum yield (PLQY) measurements revealed a PLQY value of 0.7% for 3.4 nm CIS NCs, both in a colloidal dispersion and in a NC film (Figure S4). Low PLQY values around 1% are typical for ternary nanocrystals.^{1–4} The size of the NCs was established from the PL peak position because the low TEM contrast does not allow for a reliable size determination (Figure S2), and a detailed size *versus* PL maximum relation for CIS NCs was presented by Li *et al.*⁶ These CIS NCs were used in the spectroelectrochemistry measurements discussed in the rest of this work.

***In Situ* Spectroelectrochemistry.** Spectroelectrochemistry is a powerful tool to study charge injection into semiconductor nanomaterials because it allows the probing of the optical properties while electrons are injected into and extracted from the NC film.^{22–24} Spectroelectrochemical absorption measurements give valuable information on the position of the band edges with respect to vacuum²⁵ and allow the determination of the number of electrons injected and extracted in and from the band edges, respectively.^{26,27} Therefore, we performed *in situ* absorption spectroscopy during electrochemical charging of CIS NC films in a wide potential window, ranging from -2.5 to $+2.0$ V *versus* Ag PRE (Figure 2). A clear reduction feature is observed around -1.8 V as well as an oxidation peak around $+0.6$ V. Typically, these

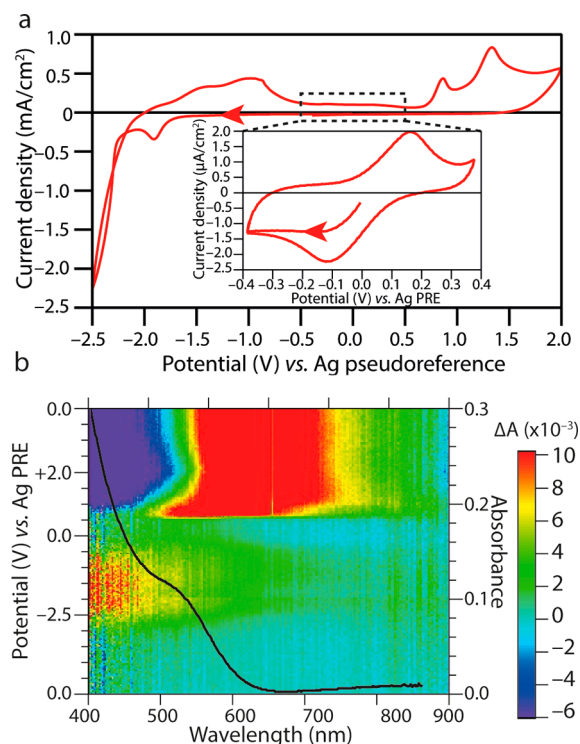


Figure 2. Cyclic voltammetry and differential absorbance. (a) Cyclic voltammogram between -2.5 to $+2.0$ V for 2.9 nm CIS NCs, showing irreversible reduction and oxidation features. Reversible features were only observed in a narrow potential window of ~ -0.4 to $\sim +0.4$ V *vs* Ag PRE (inset). (b) Differential absorbance plots as a function of applied potential. No changes in absorbance are observed at negative applied potentials despite a small induced absorbance at -2.5 V, originating from charging of the ITO substrate. At positive potentials exceeding $+0.5$ V, irreversible absorption changes are observed due to deterioration of the NC film. For comparison, the steady-state absorption is plotted on top of the differential absorbance plot (black line, right axis).

features are assigned to the band edges of the CIS NC^{2,28–31} because the measured electrochemical band gap (2.4 V) is of the same order as the optical band gap (550 nm, 2.3 eV). However, the combination of cyclic voltammetry with *in situ* absorption measurements used here (Figure 2b) reveals no changes in absorption at these reduction and oxidation peaks, suggesting that these features cannot be assigned to the CB and VB edges because state filling of the band edges would result in a decrease in absorption.^{32,33} Furthermore, the NCs deteriorate irreversibly at positive potentials, indicated by an overall, irreversible decrease in absorption (Figure 2b). In contrast, we find that for a smaller potential window (between -0.4 and $+0.4$ V) the CVs are fully reversible, and no deterioration of the NCs occurs (inset of Figure 2a). Therefore, we focus on this smaller potential window for the remainder of this paper.

In addition to *in situ* absorption spectroscopy, we also performed *in situ* photoluminescence spectroscopy^{34,35} during the electrochemical charging of 5.5 nm CuInS_2 nanocrystals (Figure 3). The same measurements were performed on the three other sizes of CIS NCs (Figures S5–7). The cyclic voltammogram (CV, Figure 3a) shows a positive current at an applied potential of ~ 0.3 V *versus* Ag PRE, indicative of electron extraction from the working electrode. Again, the

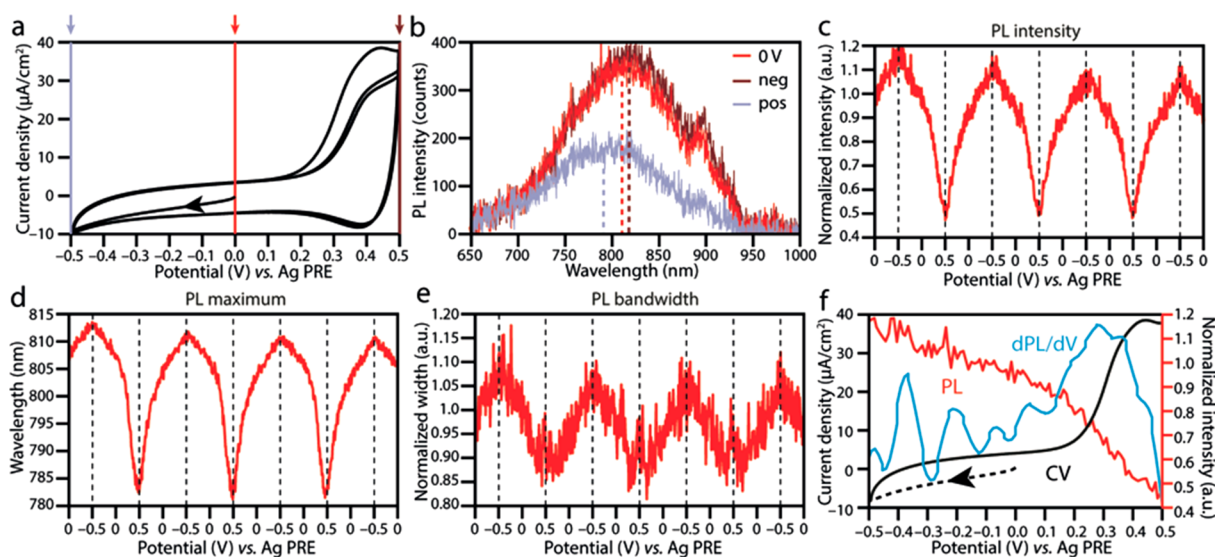


Figure 3. *In situ* photoluminescence spectroelectrochemistry measurements on CIS NCs. (a) Cyclic voltammogram showing electron injection and extraction into and from a CIS NC film. The colored arrows indicate the potentials at which the PL spectra in panel b were recorded. (b) PL spectra at the open circuit potential V_{oc} (red line), -0.5 V (brown line), and $+0.5$ V (blue line). The dashed lines indicate the PL maxima. (c–e) Temporal evolution plots of (c) the PL intensity, (d) the PL maximum, and (e) PL bandwidth. (f) The derivative of the PL change as a function of the applied potential (dPL/dV , blue line) shows that there is an offset between the maximum current density ($+0.4$ V vs Ag PRE, black line) and the maximum change in PL ($+0.3$ V vs Ag PRE). The variation in PL intensity as a function of applied potential is plotted for comparison (red line).

differential absorption spectra are devoid of any features in this potential window (Figure S8), indicating that no electrons are injected into and extracted from the band edges at these applied potentials.^{25,36} Possibly, in the potential window studied here (Figure 3a, -0.5 to $+0.5$ V versus Ag PRE) electrons are only injected and extracted into and from in-gap trap states, respectively,²² or other side reactions, like the oxidation and reduction of surface ligands, might occur.

Because the radiative recombination in ternary CIS NCs involves midgap trap states (Figure 1), *in situ* photoluminescence spectroscopy will give valuable insights into the influence of additional charges on the radiative recombination in this material. We find that at the maximum negative applied potential (-0.5 V), the PL band is slightly shifted to longer wavelengths (*i.e.*, lower energies) and has increased in intensity (Figure 3b, red line at -0.02 V, open circuit potential, V_{oc} and brown line at -0.5 V versus Ag PRE). The opposite is observed for the maximum positive applied potential: the PL peak maximum has shifted considerably to shorter wavelengths (*i.e.*, higher energy) and has decreased in intensity (Figure 3b, red line at V_{oc} and blue line at $+0.5$ V versus Ag PRE).

We follow the evolution of the three main characteristics of the PL band as a function of the applied potential: the intensity (Figure 3c), position of the maximum (Figure 3d), and the PL bandwidth (Figure 3e). These plots show a clear correlation between the characteristic PL features and the applied potential. At negative applied potentials (electron injection), the PL maximum red shifts slightly by ~ 6 nm (Figure 3d), whereas the intensity increases by $\sim 15\%$ (Figure 3c). Furthermore, the PL band broadens by $\sim 10\%$ (Figure 3e). This implies that the absolute PLQY increases from 0.7% to 0.8%. At positive applied potentials (electron extraction), the optical changes are more pronounced: the PL maximum blue shifts by ~ 25 nm, the intensity drops by over 50% and the PL band narrows by $\sim 15\%$, resulting in a PLQY decrease from 0.7% at V_{oc} to 0.4% at $+0.5$ V versus Ag PRE. We observe the

same trends for the other sizes of CIS NCs (Figure S5–7). The small, steady decline of the PL intensity after a full CV cycle (Figure 3c) is attributed to laser damage due to the focused laser spot (Figure S9).

It is tempting to associate the observed changes in the PL characteristics to the oxidation and reduction waves seen in the CV (Figure 3a). However, we find that the maximum change in PL intensity (analyzed by taking the derivative of the PL intensity as a function of the applied potential, dPL/dV ; Figure 3f) does not correspond to the highest current density for all CIS NCs studied here. As shown in Figure S10, for all investigated sizes, the maximum change in PL occurs at significantly more negative potentials than the maximum current observed in the CVs. Therefore, we infer that the observed oxidation and reduction waves in the CVs actually originate from other species in the system than the radiative recombination centers, such as bound surface thiolate ligands.^{37–39} In fact, the potential of the observed oxidation wave with respect to vacuum ($+0.45$ V versus Ag PRE corresponds to -5.2 V versus vacuum) is close to the potential of the oxidation of surface thiolate ligands on colloidal CdTe NCs (-5.15 V versus vacuum).³⁹ Furthermore, it is likely that the ratio between surface thiolate ligands and internal Cu^+/Cu^{2+} states is large, which makes the current corresponding to the oxidation of bound thiolates dominant in the CV scans.

Interestingly, we find a good agreement between the line width of the PL (between 220 and 250 meV) and the width of the variation in PL intensity as a function of applied potential (~ 250 meV; see Figure S10). This suggests that the observed PL line width is indeed due to a relatively broad distribution of Cu^+/Cu^{2+} states, as was inferred above (Figure 1c). Our results thus show that the combination of cyclic voltammetry with optical measurements is crucial to assign the observed electrochemical features to specific characteristics of the NCs under study.

Mechanism and Model for Radiative Recombination in Ternary CuInS_2 Nanocrystals. In a detailed spectroscopic study by Berends *et al.*, it was suggested that in “bright” NCs holes trap very rapidly (less than a picosecond) and recombine radiatively with conduction band electrons, while in “dark” NCs, both charge carriers are trapped and recombine non-radiatively.¹³ Recently, Brovelli and co-workers reported on reduced electron trapping by raising the Fermi level, which resulted in brighter CIS NCs.¹⁷ Indeed, the filling of trap states, which reduces the electron trapping probability, is a possible explanation for the increase in PL efficiency upon raising the Fermi level, as was observed previously by our group in films of CdTe NCs.^{22,40} However, filling of electron traps is incompatible with the other trends observed in our current experiments, *i.e.*, the red shift of the PL and the broadening of the PL band upon electron injection. Because the radiative recombination in ternary CIS NCs is established to be from the conduction band edge toward a localized hole state within the band gap, reduced electron trapping due to a rise of the Fermi level will only affect the PL intensity and not the PL energy and bandwidth, as observed here. Our results therefore show that the trap level that is filled and emptied electrochemically is directly involved in the radiative recombination process.

Our *in situ* PL spectroelectrochemistry experiments can be very well explained by oxidation of Cu^+ into Cu^{2+} , which results in “dark” NCs, as was suggested in Figure 1c. To verify that electrochemical oxidation of CIS NCs indeed results in an increase in Cu^{2+} cations, we measured the Cu K-edge X-ray absorption near-edge spectroscopy (XANES) spectra upon application of a reducing and oxidizing potential by *in situ* X-ray absorption measurements^{41–44} and analyzed the observed features in the XANES pattern by simulating the spectra with standard FEFF and FDMES programs (Figures 4 and S11–13). From this, we attempt to correlate the observed quenching/brightening of the characteristic PL feature of CIS NCs under oxidizing and reducing conditions to the presence of Cu^{2+} cations (“dark”) and Cu^+ cations (“bright”). Our simulations show that the so-called “white line”, which is the main peak observed in the Cu K-edge XANES spectrum, decreases when a small cluster is simulated compared to the bulk CIS spectrum (Figure 4a), in line with a decrease of the ratio between internal and surface Cu atoms.⁴⁴ Interestingly, when additional positive charge is added to the simulated cluster, the “white line” increases more drastically (Figure 4a). In general, a more-intense “white line” is associated with an increase of positive charge on the absorber atom^{45,46} and thus infers an increase in the average oxidation state of the absorber atoms. When an electrochemical potential is applied, no evident variations in the pre-edge region, typically assigned to Cu^{2+} , are observed (Figure 4b). Small, but more evident, changes can be observed at the main peak (Figure 4b). This suggests that either the ratio between internal and surface Cu atoms increases⁴⁴ or that the average oxidation state of the Cu atoms >1 upon the application of an electrochemical potential (Figure 4b),^{45,46} effectively increasing the net positive charge at oxidizing potentials and decreasing the net positive charge at reducing potentials. In fact, given the low number of luminescent Cu sites that change oxidation state, as suggested by the *in situ* electrochemistry results discussed above, it will be very challenging to gain conclusive information on these Cu^{2+} sites from Cu K-edge XANES measurements to distinguish between these two possibilities. To improve this analysis, the

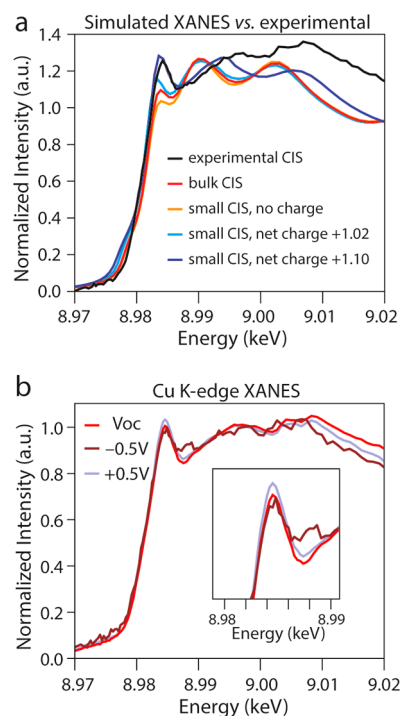


Figure 4. Simulated and experimental Cu K-edge XANES spectra. (a) Simulated XANES spectra for bulk CuInS_2 (CIS, red line), a small CIS cluster without additional charge (orange line), a small cluster with net positive charge of +1.02 (light blue line), and +1.1 (dark blue line), compared to the experimental CIS NC XANES spectrum (black line). An increase in the “white line”, which is the main peak at the edge, is observed when more internal Cu atoms are present with respect to surface Cu atoms and when the net positive charge increases. (b) *In situ* XANES spectra at open circuit potential (V_{oc} , red line), at -0.5 V vs Ag PRE (brown line), and at $+0.5$ V vs Ag PRE (light blue line), showing a small increase in the intensity of the “white line” upon the application of an oxidizing potential. The inset shows a zoomed-in view of the white line.

same measurements could be performed in fluorescence mode at the Cu L_3 -edge because this edge is more sensitive to d-type electrons that are likely involved here (electron configuration Cu^{2+} : $[\text{Ar}]3d^9$).

While the *in situ* XANES measurements on their own are not conclusive evidence of the presence of Cu^{2+} and the variation of the Cu^+ -to- Cu^{2+} ratio with changing electrochemical potential, the results are in line with the spectroelectrochemical findings presented above. Based on these combined results, we propose that we can activate “dark” NCs into “bright” NCs by injecting electrons into the CIS NCs, thereby increasing the PL intensity because more Cu^+ states are involved in the radiative recombination process. As shown in Figure 5, we propose that this occurs *via* the reduction of a “dark” Cu^{2+} defect containing CIS NC to a “bright” Cu^+ containing NC by injection of an electron, which affects not only the PL intensity but also the PL bandwidth and maximum of the ensemble due to the rise of the Fermi level within the ensemble distribution of trap states (Figure 5b). The “activated” Cu^+ can subsequently trap a photogenerated hole and, hence, contribute to radiative recombination (Figure 5c).¹³ As a consequence, the distribution of active trap states in the ensemble is broadened upon raising the Fermi level, resulting in broader PL line widths (Figure 5c). Furthermore, this shifts the PL peak position to the red side of the PL band because the separation

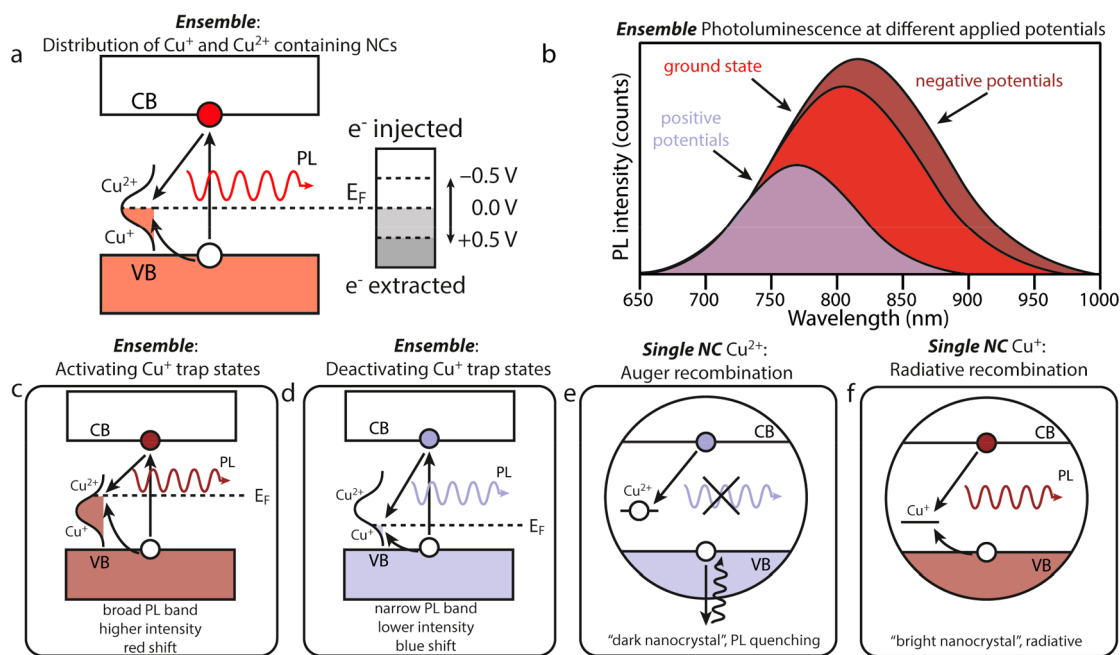


Figure 5. Recombination mechanism upon reducing and oxidizing potentials. (a) Schematic representation of radiative recombination in an ensemble of ternary CuInS_2 nanocrystals, which involves a distribution of trap states, corresponding to single Cu^+ (below the Fermi level, E_F) and Cu^{2+} (above E_F) defect states for each individual NC. Active defect states (Cu^+) within the band gap are indicated by the colored area in the trap-state distribution. (b) The distribution of trap states determines the width, position, and intensity of the PL band, depending on the ratio between NCs containing Cu^{2+} (positive potentials) and Cu^+ (negative potentials) trap states within the ensemble. The distribution of trap states can be tuned by (c) applying positive potentials vs Ag pseudoreference electrode (PRE) and (d) negative potentials vs Ag PRE. This results in (c) a shift to lower energy, broadening of the PL line width and an increase in intensity when negative potentials are applied, and (d) a shift to higher energy, narrowing of the PL line width and a decrease in intensity when positive potentials are applied by (c) activating single Cu^+ trap states and (d) deactivating single Cu^+ trap states, which is responsible for radiative recombination in ternary CuInS_2 nanocrystals. (e) Efficient Auger recombination of the electron with the excess hole (in a single electrochemically oxidized Cu^{2+} cation within a CIS NCs), and the photogenerated hole in the VB edge results in additional non-radiative recombination and, hence, quenching of the PL. (f) In the absence of a Cu^{2+} center, the single CIS NC is bright after quick localization of the photogenerated hole on the Cu^+ center and radiative recombination with the delocalized CB electron.

between the conduction band edge and the maximum of the distribution of activated defect states (Fermi level, E_F) has decreased. The opposite is observed for oxidizing potentials (Figure 5d).

Our observations are in contrast to the observations of Klimov and co-workers, who recently reported on the presence of both active Cu^{2+} and Cu^+ luminescent centers in the ground state, depending on the Cu-to-In ratio in the CIS NCs.^{19,20} They state that Cu^{2+} defects also display photoluminescence but that a separate hole-trapping state is necessary for the Cu^{2+} state to be active.²⁰ Furthermore, they suggest that if the photogenerated hole is not trapped, band-edge recombination will out-compete the radiative recombination transition to the Cu^{2+} cation.²⁰ We note that band edge recombination is not observed in our experiments. In fact, when an oxidizing potential is applied, the suggested hole traps that render Cu^{2+} centers emissive²⁰ will be depleted of electrons and, hence, can no longer trap photogenerated holes. One could expect that this results in enhancement of the band edge recombination,²⁰ which is not what we observe when oxidizing potentials are applied. We suggest that in the case of empty hole trap states, an Auger-assisted trapping process of the conduction band electron to the in-gap Cu^{2+} center, which excites the valence band hole to a deeper energy level, will open up. This then results in nonradiative recombination and the absence of both band-edge and trap-state emission. However, as we discuss in more detail below, we believe that this non-radiative trap-

assisted Auger recombination pathway is also present in the ground state. In this scenario, the $\text{Cu}^+/\text{Cu}^{2+}$ emissive state is the only state required to explain the PL dependence on the applied potential.

We suggest that the presence of Cu^{2+} cations renders the NC “dark”, due to efficient trap-assisted Auger recombination. As shown in Figure 5e, this process involves a conduction band electron that is trapped nonradiatively on the Cu^{2+} defect, while the energy is transferred to the photogenerated valence band hole. We note that this is similar to our earlier observation that electrons trap rapidly to deep defect states near the VB edge in CdTe NCs via Auger excitation of photogenerated holes²² and also similar to trap-assisted Auger recombination of excess CB electrons in Cu^+ -doped CdSe/CdS NCs.⁴⁷

If each NC contains a large number of luminescent Cu^+ trap states, then oxidizing a fraction of those trap states would leave many active Cu^+ states in the band gap on which the photogenerated hole can localize and avoid Auger recombination, given that hole localization is much faster than Auger recombination. This would suggest that the NCs remain luminescent. However, we have no indication of the rate of Auger recombination. For our model to be consistent, we thus need to assume that each NC contains only a few photoactive Cu-based traps. This is supported by the observation that the observed electrochemical peaks do not result in the variations in the PL characteristics, which suggests that small

concentrations of $\text{Cu}^+/\text{Cu}^{2+}$ states are oxidized and reduced (Figure 3f). For CdTe NCs, we have observed a similar trap-assisted Auger recombination process as inferred here, which takes place within a picosecond,²² on a similar time scale as has been reported for hole trapping in CIS NCs.¹³ Thus, there could be an effective competition between hole trapping and Auger recombination that changes depending on the relative number of available Cu^+ levels for hole trapping, which is responsible for the change of the PLQY with electrochemical potential. Once all luminescent Cu traps in a NC are oxidized to Cu^{2+} , the NC turns dark completely. This suggests that we are switching some NCs into the “off” state by oxidizing the “active” Cu^+ states into “inactive” Cu^{2+} states. We specifically note that it thus takes only one, or at most a few, electrochemically oxidized Cu^{2+} cations to turn the NC dark.

These results indicate that the distribution of active hole-trap states (Cu^+ defects) within the ensemble correlates directly to the bandwidth of the PL, and that this distribution can be reversibly tuned by electrochemical methods. The hypothesis from these *in situ* photoluminescence spectroelectrochemistry measurements is therefore that dark states correspond to Cu^{2+} defects and bright states to Cu^+ defects. However, direct evidence that Cu defects are involved in the photoluminescence and that it is their oxidation state that changes in the electrochemical scans is still lacking. Previously, it has only been inferred from the position of the oxidation and reduction waves observed in the CVs^{2,20} because the potentials are close to what has been measured in water for the $\text{Cu}^+/\text{Cu}^{2+}$ couple.⁴⁸ We note that the $\text{Cu}^+/\text{Cu}^{2+}$ reduction and oxidation in CIS NCs is likely different from that of dissolved ions in water.⁴⁸ Furthermore, as was discussed above, there is an offset between the maximum current density and the maximum change in PL of ~ 0.1 eV (Figure S10), which leads to the conclusion that the observed oxidation/reduction waves do not correspond to the luminescent $\text{Cu}^+/\text{Cu}^{2+}$ redox couple but possibly to surface thiolate ligands.^{37–39} In addition, we wish to note that the concentration of Cu^{2+} cations in the ensemble is likely very low. If 1 out of 100 Cu cations in a CIS NC is a Cu^{2+} , and not all CIS NCs contain a Cu^{2+} , the ensemble Cu^{2+} concentration will be much lower than 1%. Therefore, elemental analysis techniques, such as *in situ* XANES (as attempted here), will possibly have insufficient sensitivity for Cu^{2+} to deconvolute the Cu^{2+} and Cu^+ signals. However, by combining *in situ* electrochemistry with photoluminescence measurements we are able to probe even small variations in the oxidation state because the redox couple is directly involved in the radiative recombination process.

One open question is exactly where these $\text{Cu}^{2+}/\text{Cu}^+$ defect states are located. The electrochemical potential of these $\text{Cu}^{2+}/\text{Cu}^+$ defect states is likely different from the other lattice Cu^+ cations within a CIS NC. Due to the highly localized nature of these states, their energy is easily perturbed by the presence of surface defects or lattice charges, as predicted in a recent density functional theory (DFT) study,⁴⁹ leading to a variable energy of the localized state within the band gap, which causes the ensemble broadening. The fact that heteroepitaxial shell overgrowth with a wider band gap semiconductor results in an increase in PLQY and similar broad-band PL features as bare CIS NCs indicates that these defect states are not located at the surface of the NCs, meaning they should be internal defects.^{6,7,50} As suggested by the same DFT study, the emissive Cu^+ centers could be located at Cu_{In} anti-sites or interstitial positions or on lattice sites adjacent to an impurity dopant,

such as an ion vacancy, or the NC surface.⁴⁹ Our results provide a model that correlates the oxidation state of the Cu cations involved in the radiative transition to the optical properties in ternary nanocrystals and also offer additional tools to tune the characteristic features of this interesting class of materials.

CONCLUSIONS

In conclusion, we probe and tune the distribution of Cu^+ and Cu^{2+} trap states in ternary CuInS_2 nanocrystals by *in situ* photoluminescence spectroelectrochemistry. We establish that the width of the “bright” Cu^+ trap-state distribution in the ensemble correlates with the PL line width, which we can tune by electron injection or extraction. Electron injection and extraction also affect the PL peak position, shifting it to lower energy in the case of electron injection and higher energy when electrons are extracted. Finally, the PL increases in intensity and broadens when electrons are injected, whereas it decreases in intensity and becomes narrower when electrons are extracted. Based on these findings, we propose that efficient hole trapping on Cu^+ defects is crucial for “bright” CIS NCs. Efficient hole trapping can be activated by injecting electrons into the “dark” defect states (Cu^{2+}), thereby also broadening the distribution of active trap states (Cu^+) within the ensemble of CIS NCs. Furthermore, we find that electrochemical oxidation of a Cu^+ -related trap state into Cu^{2+} , reduces the PL intensity due to an efficient Auger recombination pathway of the photogenerated valence band hole. Our model shows a direct correlation between trap-state distribution and PL line width, peak maximum and intensity, and the oxidation state of the Cu-related defects, which contributes to understanding the characteristic features of ternary NCs (*i.e.*, low quantum yield, large global Stokes shift, and broad PL line width) and provides a toolkit to control and manipulate these characteristics for the envisioned application.

METHODS

Materials. Copper(I) iodide (CuI , 99.999%, Sigma-Aldrich), indium acetate (InAc_3 , 99.99%, Sigma-Aldrich), 1-dodecanethiol (DDT, >98%, Sigma-Aldrich), ethanedithiol (EDT, >98%, Sigma-Aldrich), indium-doped tin oxide substrates (ITO, ~ 25 nm film thickness, $R_{\text{sq}} \leq 120 \Omega/\text{cm}^2$, PGO Germany), thin Indium-doped tin oxide substrates (ITO, ~ 25 nm film thickness, total substrate thickness of $\sim 100 \mu\text{m}$, $R_{\text{sq}} \leq 120 \Omega/\text{cm}^2$, PGO Germany), lithium perchlorate (LiClO_4 , 99.99%, Sigma-Aldrich), and ferrocene (Fc, 98%, Sigma-Aldrich) were used. Anhydrous solvents (methanol, 99.8%; butanol, 99.8%; and toluene, 99.8%) and acetonitrile (99.99%) were all purchased from Sigma-Aldrich. Acetonitrile was dried before use in an Innovative Technology PureSolv Micro column. All other chemicals were used as received.

Synthesis of CuInS_2 Nanocrystals. The CuInS_2 (CIS) nanocrystals (NCs) were synthesized according to a protocol from literature.⁶ In a typical synthesis, 1 mmol indium acetate (0.292 g) and 1 mmol copper(I) iodide (0.190 g) were mixed in a three-necked flask with 10 mL 1-dodecanethiol (DDT). The mixture was degassed and purged with nitrogen (N_2) three times under stirring. The flask was heated to 100 °C until a clear solution had formed and subsequently heated further to 230 °C. The NCs were grown for varying growth times to obtain colloidal dispersions with different sizes of CIS NCs (growth times of 5, 12, 15, and 30 min). The flask was cooled with an air gun to below 100 °C and quenched by the addition of 5 mL of anhydrous toluene. The NCs were precipitated in a 1:1:1 mixture of crude solution/methanol/butanol upon centrifugation at 3000 rpm for 10 min. Afterward, the supernatant was

discarded and the NCs were redispersed in toluene. These washing steps were repeated three times.

CuInS₂ NC film Preparation. The CuInS₂ (CIS) NC films were prepared in a N₂-purged glovebox using a dip coater from Nima Technology. Indium-doped tin oxide (ITO) covered glass plates were consecutively dipped for 30 s in a concentrated colloidal dispersion of CIS NCs, a 14 v% solution of ethanedithiol (EDT) ligands in methanol to cross-link the NCs, and a methanol solution to remove the excess, unbound ligands. The above-mentioned procedure was repeated 10 times to obtain sufficiently thick NC films. Afterward, the plates were dried for an hour inside the glovebox. The CIS NC films on ITO were used as working electrode (WE) in the spectroelectrochemical measurements described below.

(Spectro)electrochemistry. The (spectro)electrochemical experiments were performed in a three electrode electrochemical cell, consisting of a Ag wire pseudoreference electrode (PRE), a platinum (Pt) plate counter electrode (CE), and the above-mentioned CIS-ITO WE. All experiments were performed inside a N₂-purged glovebox. The supporting electrolyte was 0.1 M lithium perchlorate (LiClO₄) in acetonitrile solution. A PGSTAT128N Autolab potentiostat was used to regulate the potential and measure the current. Cyclic voltammograms were recorded with a scan speed of 0.05 V/s. The Ag-wire PRE was calibrated with a ferrocene/ferrocenium redox couple between applied potentials of -1.0 and +1.5 V at a scan rate of 0.05 V/s (Ag PRE *versus* vacuum: -4.71 V).^{26,51} During the electrochemical charging, differential absorbance spectra were recorded on a USB2000+ spectrometer (Ocean Optics, range 200 to 1025 nm) and detected with optical fibers. The white light source was a DH-2000 deuterium halogen UV-vis-NIR Lightsource from Ocean Optics. A background correction was made with a blank ITO plate prior to measurements. A photograph and a schematic of the setup can be found in Figure S14.

In Situ Photoluminescence Spectroelectrochemistry. The same electrochemical cell and detector as described above were used for the *in situ* photoluminescence experiments. The sample was excited with a 405 nm Thorlabs laser under a 45° angle with respect to the sample and focused onto the sample with a lens. The PL was detected perpendicular to the sample. Furthermore, the PL was focused onto the detection fiber by two lenses. A photograph and schematic of the setup can be found in Figure S15.

Ex Situ Optical Spectroscopy. *Ex situ* optical measurements were performed on diluted colloidal dispersions in toluene. Samples were prepared by diluting the stock solution of washed NCs with anhydrous toluene under nitrogen. Samples were stored in closed quartz cuvettes. Absorption spectra were measured on a double-beam PerkinElmer Lambda 900 UV-vis spectrometer. Photoluminescence spectra and photoluminescence quantum yield (PLQY) measurements were recorded on an Edinburgh Instruments FLS980 spectrofluorimeter equipped with a 450 W xenon lamp as excitation source and double grating monochromators.

X-ray Diffractometry. XRD measurements were performed with a Bruker D8 DISCOVER, equipped with a Cu K- α X-ray source ($\lambda = 1.5418 \text{ \AA}$), under grazing incidence conditions (angle of incidence of 1°), to minimize the contribution from the ITO substrate. The CIS-ITO electrode described above was used for the XRD measurements.

X-ray Absorption Near-Edge Spectroscopy and Extended X-ray Absorption Fine Structure. Cu K-edge (8.979 keV) XANES and EXAFS spectra of the solid and liquid samples containing CuInS₂ nanocrystals were collected at the Dutch-Belgian Beamline (DUBBLE) at the European Synchrotron Radiation Facility (ESRF).⁵² The energy of the X-ray beam was tuned by a double-crystal monochromator operating in fixed-exit mode using a Si(111) crystal pair. The samples were measured at 25 °C in 1 mm quartz capillaries (for solutions), and the CIS-ITO WE described above was used as solid sample. EXAFS spectra were collected in transmission mode using Ar/He-filled ionization chambers at ambient temperature and pressure. The XANES spectra were collected in an electrochemical cell designed for *in situ* X-ray absorption measurements in transmission mode (Figure S12). The optical path length through the electrolyte solution was kept minimal (~3 mm) to ensure high

intensity. Thin ITO-quartz plates were used to avoid X-ray absorption by the quartz.

Simulations of XANES Spectra. The results of the simulations of copper atoms are based on the theoretical approach implemented in the relativistic, self-consistent FEFF8 code. The cluster size of the multiple scattering calculations is specified by the FMS card and that for the self-consistent field calculations by the SCF card in the input file. Default values of other input options were used. The only nonstandard input to FEFF8 were the EXCHANGE card (EXCHANGE 0 0 0.2), indicating that the calculations are carried out using the Hedin-Lundqvist/Dirac-Hara plasmon pole self-energy, without shifts and with some additional broadening (0.20 eV), and the INTERSTITIAL card (0 2.83) due to the interstitial potential useful for open systems. These parameters usually agree better with experimental results.⁵³

ASSOCIATED CONTENT

Supporting Information

The Supporting Information is available free of charge on the ACS Publications website at DOI: 10.1021/acsnano.8b05843.

Figures showing steady-state UV-vis absorption and photoluminescence spectra for different sizes of CIS NCs, transmission electron microscopy and powder X-ray diffractogram results, *in situ* photoluminescence spectra and cyclic voltammograms, differential absorbance plots, dPL/dV *vs* current density plots, XANES pattern for CIS NCs in solution, a photograph and schematic of the *in situ* X-ray absorption electrochemical cell, and photographs and schematics of the spectroelectrochemical setups; additional details on photoluminescence quantum yield measurements (PDF)

AUTHOR INFORMATION

Corresponding Authors

*E-mail: W.vanderStam@tudelft.nl

*E-mail: A.J.Houteven@tudelft.nl

ORCID

Ward van der Stam: 0000-0001-8155-5400

Solrun Gudjonsdottir: 0000-0002-4793-8747

Nicholas Kirkwood: 0000-0002-7845-7081

Arjan J. Houteven: 0000-0001-8328-443X

Notes

The authors declare no competing financial interest.

ACKNOWLEDGMENTS

A.J.H. acknowledges support from the European Research Council Horizon 2020 ERC grant agreement no. 678004 (Doping on Demand). DUBBLE beamline is acknowledged for the granted beam time under proposal number 26-01-1125. The authors are very grateful to Dimitri de Roos (TU Delft) and Peter van den Beld (Utrecht University) for the *in situ* XANES cell preparation.

REFERENCES

- (1) Aldakov, D.; Lefrançois, A.; Reiss, P. Ternary and Quaternary Metal Chalcogenide Nanocrystals: Synthesis, Properties and Applications. *J. Mater. Chem. C* **2013**, *1*, 3756–3776.
- (2) Sandroni, M.; Wegner, K. D.; Aldakov, D.; Reiss, P. Prospects of Chalcopyrite-Type Nanocrystals for Energy Applications. *ACS Energy Lett.* **2017**, *2*, 1076–1088.
- (3) van der Stam, W.; Berends, A. C.; de Mello Donega, C. Prospects of Colloidal Copper Chalcogenide Nanocrystals. *ChemPhysChem* **2016**, *17*, 559–581.

- (4) Kolny-Olesiak, J.; Weller, H. Synthesis and Application of Colloidal CuInS₂ Semiconductor Nanocrystals. *ACS Appl. Mater. Interfaces* **2013**, *5*, 12221–12237.
- (5) Wu, K.; Li, H.; Klimov, V. I. Tandem Luminescent Solar Concentrators Based on Engineered Quantum Dots. *Nat. Photonics* **2018**, *12*, 105–110.
- (6) Li, L.; Pandey, A.; Werder, D.; Khanal, B. P.; Pietryga, J. M.; Klimov, V. I. Efficient Synthesis of Highly Luminescent Copper Indium Sulfide-Based Core/Shell Nanocrystals with Surprisingly Long-Lived Emission. *J. Am. Chem. Soc.* **2011**, *133*, 1176–1179.
- (7) de Trizio, L.; Prato, M.; Genovese, A.; Casu, A.; Povia, M.; Simonutti, R.; Alcocer, M. J. P.; D'Andrea, C.; Tassone, F.; Manna, L. Strongly Fluorescent Quaternary Cu–In–Zn–S Nanocrystals Prepared from Cu_{1-x}InS₂ Nanocrystals by Partial Cation Exchange. *Chem. Mater.* **2012**, *24*, 2400–2406.
- (8) van der Stam, W.; Berends, A. C.; Rabouw, F. T.; Willhammar, T.; Ke, X.; Meeldijk, J. D.; Bals, S.; de Mello Donega, C. Luminescent CuInS₂ Quantum Dots by Partial Cation Exchange in Cu_{2-x}S Nanocrystals. *Chem. Mater.* **2015**, *27*, 621–628.
- (9) Mu, L.; Wang, F.; Sadtler, B.; Loomis, R. A.; Buhro, W. E. Influence of the Nanoscale Kirkendall Effect on the Morphology of Copper Indium Disulfide Nanoplatelets Synthesized by Ion Exchange. *ACS Nano* **2015**, *9*, 7419–7428.
- (10) Kruszynska, M.; Borchert, H.; Parisi, J.; Kolny-Olesiak, J. Synthesis and Shape Control of CuInS₂ Nanoparticles. *J. Am. Chem. Soc.* **2010**, *132*, 15976–15986.
- (11) van der Stam, W.; Bladt, E.; Rabouw, F. T.; Bals, S.; de Mello Donega, C. Near-Infrared Emitting CuInSe₂/CuInS₂ Dot Core/Rod Shell Heteronanorods by Sequential Cation Exchange. *ACS Nano* **2015**, *9*, 11430–11438.
- (12) Whitham, P. J.; Marchioro, A.; Knowles, K. E.; Kilburn, T. B.; Reid, P. J.; Gamelin, D. R. Single-Particle Photoluminescence Spectra, Blinking, and Delayed Luminescence of Colloidal CuInS₂ Nanocrystals. *J. Phys. Chem. C* **2016**, *120*, 17136–17142.
- (13) Berends, A. C.; Rabouw, F. T.; Spoor, F. C. M.; Bladt, E.; Grozema, F. C.; Houtepen, A. J.; Siebbeles, L. D. A.; De Mello Donega, C. Radiative and Nonradiative Recombination in CuInS₂ Nanocrystals and CuInS₂-Based Core/Shell Nanocrystals. *J. Phys. Chem. Lett.* **2016**, *7*, 3503–3509.
- (14) Zang, H.; Li, H.; Makarov, N. S.; Velizhanin, K. A.; Wu, K.; Park, Y.-S.; Klimov, V. I. Thick-Shell CuInS₂/ZnS Quantum Dots with Suppressed “Blinking” and Narrow Single-Particle Emission Line Widths. *Nano Lett.* **2017**, *17*, 1787–1795.
- (15) Knowles, K. E.; Hartstein, K. H.; Kilburn, T. B.; Marchioro, A.; Nelson, H. D.; Whitham, P. J.; Gamelin, D. R. Luminescent Colloidal Semiconductor Nanocrystals Containing Copper: Synthesis, Photo-physics, and Applications. *Chem. Rev.* **2016**, *116*, 10820–10851.
- (16) Knowles, K. E.; Nelson, H. D.; Kilburn, T. B.; Gamelin, D. R. Singlet-Triplet Splittings in the Luminescent Excited States of Colloidal Cu⁺:CdSe, Cu⁺:InP, and CuInS₂ Nanocrystals: Charge-Transfer Configurations and Self-Trapped Excitons. *J. Am. Chem. Soc.* **2015**, *137*, 13138–13147.
- (17) Pinchetti, V.; Lorenzon, M.; McDaniel, H.; Lorenzi, R.; Meinardi, F.; Klimov, V. I.; Brovelli, S. Spectro-Electrochemical Probing of Intrinsic and Extrinsic Processes in Exciton Recombination in I–III–VI₂ Nanocrystals. *Nano Lett.* **2017**, *17*, 4508–4517.
- (18) Whitham, P. J.; Knowles, K. E.; Reid, P. J.; Gamelin, D. R. Photoluminescence Blinking and Reversible Electron Trapping in Copper-Doped CdSe Nanocrystals. *Nano Lett.* **2015**, *15*, 4045–4051.
- (19) Rice, W. D.; McDaniel, H.; Klimov, V. I.; Crooker, S. A. Magneto-Optical Properties of CuInS₂ Nanocrystals. *J. Phys. Chem. Lett.* **2014**, *5*, 4105–4109.
- (20) Fuhr, A. S.; Yun, H. J.; Makarov, N. S.; Li, H.; McDaniel, H.; Klimov, V. I. Light Emission Mechanisms in CuInS₂ Quantum Dots Evaluated by Spectral Electrochemistry. *ACS Photonics* **2017**, *4*, 2425–2435.
- (21) Houtepen, A. J.; Hens, Z.; Owen, J. S.; Infante, I. On the Origin of Surface Traps in Colloidal II-VI Semiconductor Nanocrystals. *Chem. Mater.* **2017**, *29*, 752–761.
- (22) Boehme, S. C.; Azpiroz, J. M.; Aulin, Y. V.; Grozema, F. C.; Vanmaekelbergh, D.; Siebbeles, L. D. A.; Infante, I.; Houtepen, A. J. Density of Trap States and Auger-Mediated Electron Trapping in CdTe Quantum-Dot Solids. *Nano Lett.* **2015**, *15*, 3056–3066.
- (23) Chen, M.; Guyot-Sionnest, P. Reversible Electrochemistry of Mercury Chalcogenide Colloidal Quantum Dot Films. *ACS Nano* **2017**, *11*, 4165–4173.
- (24) van der Stam, W.; Gudjonsdottir, S.; Evers, W. H.; Houtepen, A. J. Switching between Plasmonic and Fluorescent Copper Sulfide Nanocrystals. *J. Am. Chem. Soc.* **2017**, *139*, 13208–13217.
- (25) Boehme, S. C.; Vanmaekelbergh, D.; Evers, W. H.; Siebbeles, L. D. A.; Houtepen, A. J. *In Situ* Spectroelectrochemical Determination of Energy Levels and Energy Level Offsets in Quantum-Dot Heterojunctions. *J. Phys. Chem. C* **2016**, *120*, 5164–5173.
- (26) Boehme, S. C.; Wang, H.; Siebbeles, L. D. A.; Vanmaekelbergh, D.; Houtepen, A. J. Electrochemical Charging of CdSe Quantum Dot Films: Dependence on Void Size and Counterion Proximity. *ACS Nano* **2013**, *7*, 2500–2508.
- (27) Zhai, Y.; Zhu, Z.; Zhou, S.; Zhu, C.; Dong, S. Recent Advances in Spectroelectrochemistry. *Nanoscale* **2018**, *10*, 3089–3111.
- (28) Chen, B.; Chang, S.; Li, D.; Chen, L.; Wang, Y.; Chen, T.; Zou, B.; Zhong, H.; Rogach, A. L. Template Synthesis of CuInS₂ Nanocrystals from In₂S₃ Nanoplates and Their Application as Counter Electrodes in Dye-Sensitized Solar Cells. *Chem. Mater.* **2015**, *27*, 5949–5956.
- (29) Sun, Y.; Qian, C.; Peng, K.; Bai, Z.; Tang, J.; Zhao, Y.; Wu, S.; Ali, H.; Song, F.; Zhong, H.; Xu, X. Recombination Processes in CuInS₂/ZnS Nanocrystals during Steady-State Photoluminescence. *Appl. Phys. Lett.* **2016**, *108*, 41106.
- (30) Zhong, H.; Lo, S.; Mirkovic, T.; Li, Y.; Ding, Y.; Scholes, G. D.; Li, Y. Noninjection Gram-Scale Synthesis of Monodisperse Pyramidal CuInS₂ Nanocrystals and Their Size-Dependent Properties. *ACS Nano* **2010**, *4*, 5253–5262.
- (31) Akkerman, Q. A.; Genovese, A.; George, C.; Prato, M.; Moreels, I.; Casu, A.; Marras, S.; Curcio, A.; Scarpellini, A.; Pellegrino, T.; Manna, L.; Lesnyak, V. From Binary Cu₂S to Ternary Cu–In–S and Quaternary Cu–In–Zn–S Nanocrystals with Tunable Composition via Partial Cation Exchange. *ACS Nano* **2015**, *9*, 521–531.
- (32) Jha, P. P.; Guyot-Sionnest, P. Photoluminescence Switching of Charged Quantum Dot Films. *J. Phys. Chem. C* **2007**, *111*, 15440–15445.
- (33) Shallcross, R. C.; Zheng, Y.; Saavedra, S. S.; Armstrong, N. R. Determining Band-Edge Energies and Morphology-Dependent Stability of Formamidinium Lead Perovskite Films Using Spectroelectrochemistry and Photoelectron Spectroscopy. *J. Am. Chem. Soc.* **2017**, *139*, 4866–4878.
- (34) Lorenzon, M.; Sortino, L.; Akkerman, Q. A.; Accornero, S.; Pedrini, J.; Prato, M.; Pinchetti, V.; Meinardi, F.; Manna, L.; Brovelli, S. Role of Nonradiative Defects and Environmental Oxygen on Exciton Recombination Processes in CsPbBr₃ Perovskite Nanocrystals. *Nano Lett.* **2017**, *17*, 3844–3853.
- (35) Brovelli, S.; Galland, C.; Viswanatha, R.; Klimov, V. I. Tuning Radiative Recombination in Cu-Doped Nanocrystals via Electrochemical Control of Surface Trapping. *Nano Lett.* **2012**, *12*, 4372–4379.
- (36) Gudjonsdottir, S.; van der Stam, W.; Kirkwood, N.; Evers, W. H.; Houtepen, A. J. The Role of Dopant Ions on Charge Injection and Transport in Electrochemically Doped Quantum Dot Films. *J. Am. Chem. Soc.* **2018**, *140*, 6582–6590.
- (37) Valero-Ruiz, E.; Gonzalez-Sanchez, M. I.; Batchelor-McAuley, C.; Compton, R. G. Halogen Mediated Voltammetric Oxidation of Biological Thiols and Disulfides. *Analyst* **2016**, *141*, 144–149.
- (38) Amelia, M.; Lincheneau, C.; Credi, A.; Silvi, S. Electrochemical Properties of CdSe and CdTe Quantum Dots. *Chem. Soc. Rev.* **2012**, *41*, 5728–5743.
- (39) Poznyak, S. K.; Osipovich, N. P.; Shavel, A.; Talapin, D. V.; Gao, M.; Eychmuller, A.; Gaponik, N. Size-Dependent Electrochemical Behavior of Thiol-Capped CdTe Nanocrystals in Aqueous Solution. *J. Phys. Chem. B* **2005**, *109*, 1094–1100.

- (40) Boehme, S. C.; Walvis, T. A.; Infante, I.; Grozema, F. C.; Vanmaekelbergh, D.; Siebbeles, L. D. A.; Houtepen, A. J. Electrochemical Control over Photoinduced Electron Transfer and Trapping in CdSe-CdTe Quantum-Dot Solids. *ACS Nano* **2014**, *8*, 7067–7077.
- (41) Hassan, A.; Zhang, X.; Liu, C.; Snee, P. T. Electronic Structure and Dynamics of Copper-Doped Indium Phosphide Nanocrystals Studied with Time-Resolved X-ray Absorption and Large-Scale DFT Calculations. *J. Phys. Chem. C* **2018**, *122*, 11145–11151.
- (42) Shearer, J.; Callan, P. E.; Szalai, V. A.; Tran, T. Cu K-Edge X-Ray Absorption Spectroscopy Reveals Differential Copper Coordination within Amyloid- β Oligomers Compared to Amyloid- β Monomers. *Chem. Commun.* **2010**, *46*, 9137–9139.
- (43) Johnson, B.; Klaer, J.; Merdes, S.; Gorgoi, M.; Hopfner, B.; Vollmer, A.; Lauermaun, I. Limitations of Near Edge X-ray Absorption Fine Structure as a Tool for Observing Conduction Bands in Chalcopyrite Solar Cell Heterojunctions. *J. Electron Spectrosc. Relat. Phenom.* **2013**, *190*, 42–46.
- (44) Hu, W.; Ludwig, J.; Pattengale, B.; Yang, S.; Liu, C.; Zuo, X.; Zhang, X.; Huang, J. Unravelling the Correlation of Electronic Structure and Carrier Dynamics in CuInS₂ Nanoparticles. *J. Phys. Chem. C* **2018**, *122*, 974–980.
- (45) Tibiletti, D.; Amieiro-Fonseca, A.; Burch, R.; Chen, Y.; Fisher, J. M.; Goguet, A.; Hardacre, C.; Hu, P.; Thompsett, D. DFT and *In Situ* EXAFS Investigation of Gold/Ceria-Zirconia Low-Temperature Water Gas Shift Catalysts: Identification of the Nature of the Active Form of Gold. *J. Phys. Chem. B* **2005**, *109*, 22553–22559.
- (46) Corma, A.; Concepción, P.; Boronat, M.; Sabater, M. J.; Navas, J.; Yacaman, M. J.; Larios, E.; Posadas, A.; López-Quintela, M. A.; Buceta, D.; Mendoza, E.; Guilera, G.; Mayoral, A. Exceptional Oxidation Activity with Size-Controlled Supported Gold Clusters of Low Atomicity. *Nat. Chem.* **2013**, *5*, 775–781.
- (47) Hughes, K. E.; Hartstein, K. H.; Gamelin, D. R. Photodoping and Transient Spectroscopies of Copper-Doped CdSe/CdS Nanocrystals. *ACS Nano* **2018**, *12*, 718–728.
- (48) Bard, A. J.; Faulkner, L. in *Electrochemical Methods: Fundamentals and Applications*; 2nd ed.; John Wiley & Sons: Hoboken, NJ, 2000.
- (49) Nelson, H. D.; Gamelin, D. R. Valence-Band Electronic Structures of Cu⁺-Doped ZnS, Alloyed Cu-In-Zn-S, and Ternary CuInS₂ Nanocrystals: A Unified Description of Photoluminescence across Compositions. *J. Phys. Chem. C* **2018**, *122*, 18124–18133.
- (50) Berends, A. C.; van der Stam, W.; Hofmann, J. P.; Bladt, E.; Meeldijk, J. D.; Bals, S.; de Mello-Donaga, C. Interplay Between Surface Chemistry, Precursor Reactivity and Temperature Determines Outcome of ZnS Shelling Reactions on CuInS₂ Nanocrystals. *Chem. Mater.* **2018**, *30*, 2400–2413.
- (51) Ruch, P. W.; Cericola, D.; Hahn, M.; Kotz, R.; Wokaun, A. On the Use of Activated Carbon as a Quasi-Reference Electrode in Non-Aqueous Electrolyte Solutions. *J. Electroanal. Chem.* **2009**, *636*, 128–131.
- (52) Nikitenko, S.; Beale, A. M.; van der Eerden, A. M.; Jacques, S. D. M.; Leynaud, O.; O'Brien, M. G.; Detollenaere, D.; Kaptein, R.; Weckhuysen, B. M.; Bras, W. Implementation of a Combined SAXS/WAXS/QEXAFS Set-up for Time-Resolved *In-Situ* Experiments. *J. Synchrotron Radiat.* **2008**, *15*, 632–640.
- (53) Rehr, J. J.; Kas, J. J.; Vila, F. D.; Prange, M. P.; Jorissen, K. Parameter-Free Calculations of X-Ray Spectra with FEFF9. *Phys. Chem. Chem. Phys.* **2010**, *12*, 5503–5513.